Raman spectra in Bi_2TeO_5 as a function of the temperature and the polarization

1998 J. Phys.: Condens. Matter 10 3659

(http://iopscience.iop.org/0953-8984/10/16/017)

J. Phys.: Condens. Matter **10** (1998) 3659–3668. Printed in the UK PII: S0953-8984(98)89926-8

Raman spectra in Bi_2TeO_5 as a function of the temperature and the polarization

R S Klein†§, W Fortin†, I Földvári‡ and G E Kugel†

† Laboratoire Matériaux Optiques à Propriétés Spécifiques, Centre Lorrain d'Optique et Electronique des Solides, Université de Metz, 2 rue E Belin, 57078 Metz Cédex 3, France

‡ Research Laboratory for Crystal Physics, HAS, Budapest, Hungary

Received 10 December 1997

Abstract. The first Raman spectroscopy results are presented on Bi_2TeO_5 single crystals in the 10 to 800 cm^{-1} frequency range for four polarization configurations. The temperature dependence of the spectra was followed and analysed in the 10–890 K region. Annealing the crystal at 873 K has led to characteristic changes in the Raman spectra that were attributed to an oxidation process leading to a Bi_2TeO_6 structure. A Raman line at 762 cm^{-1} was found to be a sensitive monitor for the oxidation.

1. Introduction

The nonlinear optical bismuth tellurite (Bi_2TeO_5) became an interesting material when its photorefractive properties were discovered [1, 2]. This crystal exhibits a long-living photorefractive signal which develops in the four-wave mixing experiments without any fixing process and lasts for years in the dark [2, 3].

Homogeneous and high-quality Bi_2TeO_5 single crystals can be grown from the melt [4]. However, the investigations of the single crystals (and previously the microcrystalline samples) have revealed anomalies in the physical properties of the material. Sharp changes were detected in the electric and dielectric properties at quite different temperatures (56 and 340 °C in [5] and [6] respectively) that were explained as a ferroelectric–paraelectric phase transition. Later investigations have rejected this assumption and attributed the physical anomalies to mobile domain structure [7], charge injections from the electrodes applied [8] and photochromic generation of point defects [3, 9]. Compositional deviations may also be responsible for the irregular properties as pointed out in [3], [10] and [11].

Bismuth tellurite crystallizes in an orthorhombic structure with space group *Abm*2. The arrangement of the atoms corresponds to a $3 \times 2 \times 1$ multiplication of a perturbed CaF_2 cell in which Te and Bi alternately fill the cation positions [12]. A main characteristic of this structure is its large number (17%) of empty oxygen positions.

The tellurium based binary oxides exist with 4^+ and 6^+ nominal Te charges (tellurites and tellurates, respectively). In general, the tellurites are stable at room temperature, their oxidation to tellurates may happen in air and the oxidation begins at temperatures characteristic for the specific tellurites (350–600 °C, see [13]). The produced tellurates then decompose again at higher temperatures, losing oxygen and recovering the tellurites. Oxidation for Bi_2TeO_5 begins at 450–500 °C and the process is complete at about 600 °C

§ E-mail address: klein@esemetz.ese-metz.fr

0953-8984/98/163659+10$19.50

[13, 14]. The decomposition of the bismuth tellurate begins at about 700 °C [13, 14]. The kinetics of the oxygen loss of Bi_2TeO_6 in the cooling period has not been investigated in detail. Following these considerations, we think that an improper reduction may occur in the actual Bi_2TeO_5 sample, which should play an important role in the physical properties of the sample.

In the present paper, the Raman spectra of the as-grown Bi_2TeO_5 samples are determined and analysed. The temperature dependence of the spectra is followed in the range from 10 to 873 K and the results obtained for several polarization configurations are compared. The thermally induced changes in the Raman spectra are measured and related to reduction/oxidation processes.

2. Experimental procedure

Bi_2TeO_5 single crystals used in these experiments were grown in air by the Czochralski technique from a Pt crucible. Technical details for growth can be found in [4]. Optical samples were prepared from the boules by cleaving along the (100) plane and by x-ray orienting, cutting and polishing in the (001) and (010) planes with respective dimensions of 2 mm × 5 mm × 6 mm.

The Raman scattering spectrometer employed in the present work consists of a Spectra-Physics argon laser (5145 Å) of 200 mW power as the excitation source and a Spex double monochromator for dispersion with a photon-counting readout system using a cooled RCA C31034 phototube for detection. The system is linked with a Datamate microprocessed controller and the data are transferred and stored on a computer. The whole system was arranged in the conventional 90° scattering geometry. The Raman spectra have been recorded in a frequency range from 10 to 800 cm^{-1} and for temperatures from 10 to 890 K.

The temperature dependence above room temperature and the thermal annealing of the samples were performed in a temperature controlled furnace attached to the Raman spectrometer, the temperature being detected with a chromel–alumel thermocouple located near the sample. The ambient atmosphere was air and the heating and cooling velocity did not exceed 20 °C min^{-1}. For the low-temperature measurements an Air Products Displex closed-circuit helium cryostat, driven by an automatic temperature indicator, was used.

At each temperature, four polarization configurations for a given diffusion plane have been studied. We present here results obtained in the YX diffusion plane (Y being the incident and X the analysed direction). Consequently, the four possible polarization configurations are $Y(ZZ)X$, $Y(XY)X$, $Y(ZY)X$ and $Y(XZ)X$ which correspond, in accordance with the space group tables, to the A_1, A_2, B_2 and B_1 modes respectively.

3. Basic Raman spectra and their interpretation

In order to determine the Raman active modes in this crystal, preliminary calculations were done by using the Porto tables [15] and the position of each atom in the unit cell [12]. These atoms have been assigned to different site symmetry as shown in table 1. The irreducible representation $\Gamma_{vibration}$ of all the modes has been calculated, taking into account the number of atoms in each site. The representation Γ_{Raman} of the Raman active modes has been deduced by subtracting the $\Gamma_{rotation}$.

The experimental Raman spectra have not evidenced all these modes because of the small intensities of a part of them and of the limited 10 to 800 cm^{-1} frequency range we studied. Nevertheless, these calculations explain the large number of structures observed in

Table 1. Calculation of the vibrational mode corresponding to the irreducible representation Γ_{Raman} in the Bi_2TeO_5 crystal. The numeration of the different atoms is the same as in [12].

Atom	Site symmetry	Porto table notation	Representation
Bi(1) Te O(1) O(3) O(5) O(6)	8d	C_1	$3A_1 + 3A_2 + 3B_1 + 3B_2$
Bi(2) Bi(3) O(4)	4c	C_s^{xz}	$2A_1 + A_2 + 2B_1 + B_2$
O(2)	4b	C_2	$A_1 + A_2 + 2B_1 + 2B_2$
		Γ_{total}	$50A_1 + 44A_2 + 52B_1 + 46B_2$
		$\Gamma_{Raman} = \Gamma_{total} - \Gamma_{rotation}\ (A_2 + B_1 + B_2)$	$50A_1 + 43A_2 + 51B_1 + 45B_2$

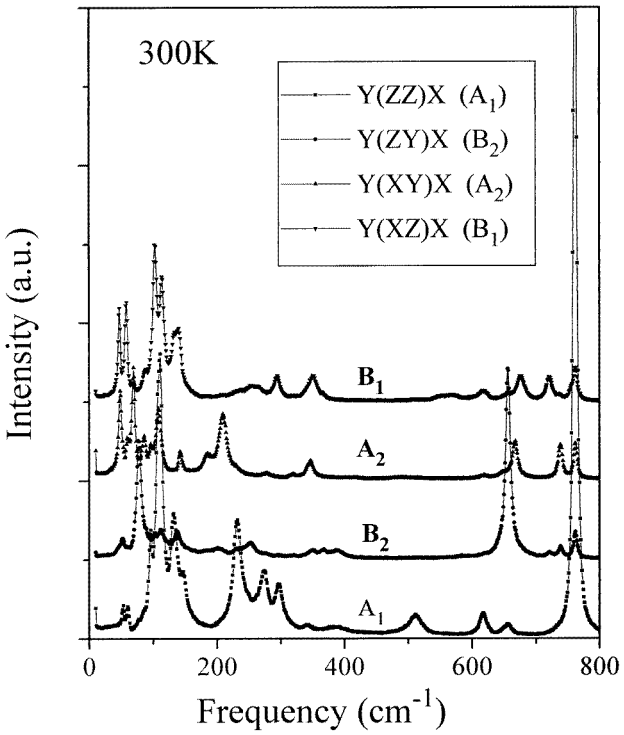

Figure 1. Raman spectra of Bi_2TeO_5 at room temperature for four polarizations: $Y(ZZ)X$, $Y(ZY)X$, $Y(XZ)X$, $Y(XY)X$.

Raman spectra.

Figure 1 shows the Raman spectra obtained at room temperature for the four polarizations described above. A strong polarization dependence of the spectra was observed. For each of the four symmetry configurations, strong line structures appear in the same range of frequencies from 10 to 200 cm^{-1}, but not at the same frequencies.

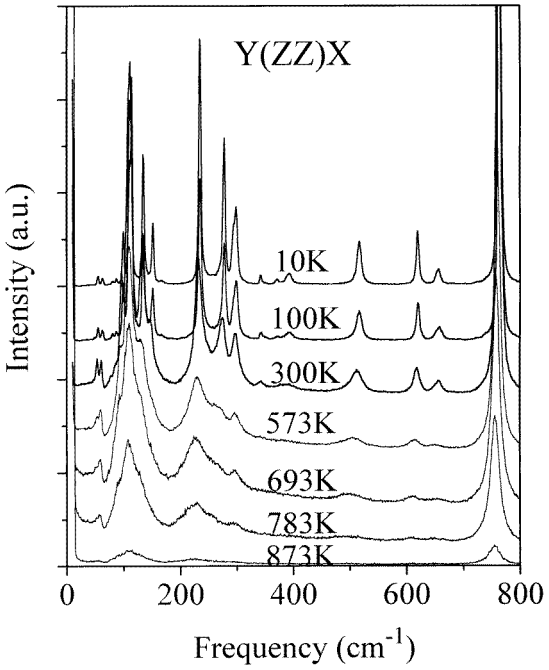

Figure 2. Variation of Raman spectra of Bi_2TeO_5 as a function of the temperature for the $Y(ZZ)X$ polarization in the range from 10 to 873 K.

The most intense line structures between 200 and 300 cm^{-1} are related specifically to the A_1 and A_2 symmetry modes. Two other important line structures were observed around 660 and 770 cm^{-1} which correspond to the B_2 and A_1 symmetry modes, respectively.

The temperature dependence of the Raman spectra in the $Y(ZZ)X$ configuration is shown in figure 2 for the 10 to 873 K range. Only slight changes appeared in the line frequencies as a function of the temperature (see figure 3 for selected lines). On the other hand, remarkable decreases of the line intensities were observed at temperatures higher than 873 K.

The temperature dependence of the four polarized Raman spectra has been analysed by fitting the experimental spectra by a damped harmonic oscillator model with the following spectral response function (for first-order Stokes Raman scattering):

$$I(\omega) = \frac{1}{(1-\exp(-\hbar\omega/k_BT))}\sum_i \frac{S_i\Gamma_i\omega\omega_i^2}{(\omega^2-\omega_i^2)^2+\Gamma_i^2\omega^2}$$

where ω_i and Γ_i correspond respectively to the mode frequency and half-width of the ith phonon. S_i is the strength of the oscillator (in arbitrary units), k_B is the Boltzmann constant and T is absolute temperature.

The behaviours as a function of temperature of the main lines belonging to the A_1, A_2, B_1 and B_2 symmetries are reported in figure 3.

Knowing the complexity of the crystalline structure of Bi_2TeO_5 [11] as well as of the Bi and Te ions surroundings and bonds with the oxygen ions, the assignment of the Raman structures to identified vibrational motions is rather difficult and constitutes a work in itself. Since the present paper is more specifically devoted to investigation of the thermal

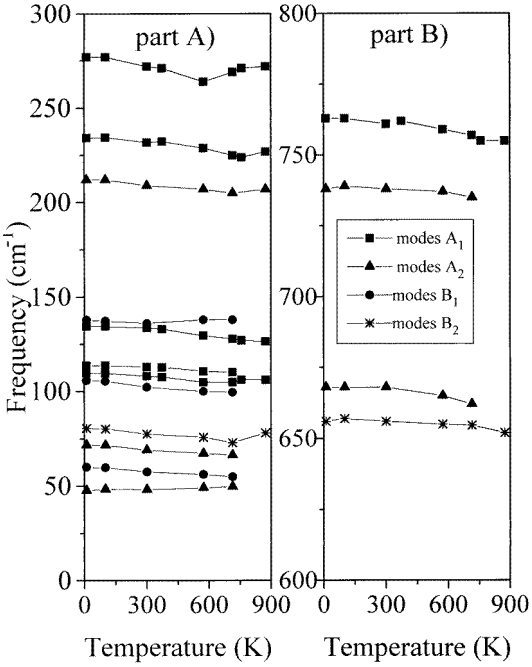

Figure 3. Temperature dependence of the frequency of the most intense line structures in four polarization configurations.

annealing, we reserve the assignment study to a forthcoming paper.

Since the frequency of the individual peaks remained almost unchanged throughout the spectra for all four polarization arrangements, we cannot verify the early assumptions of a phase transition in the investigated 10 to 873 K temperature region. The strong decrease of the line intensities at high temperatures (figure 2) should be explained in another way. According to the thermoanalytical results in [13] and [14], this decrease may be related to the oxidation of the crystal.

4. Raman spectra of thermally annealed crystals

The crystal growth from the melt includes a cooling process in which the Bi_2TeO_5 crystals pass through the temperature range where the oxidized Bi_2TeO_6 composition is the thermodynamically stable form. Depending on the kinetic situation, this may result in residues of the oxidized state in the as-grown crystals at room temperature. The Raman spectra are expected to be sensitive for these oxidation deviations. The thermal annealing experiments are designed to induce changes in the oxidation status of the crystals. We assume that, for single crystals, the efficient, bulk oxidation began at higher temperatures than those described for powder or microcrystalline samples [13, 14].

The samples were heated to specific temperatures at which oxidative/reductive changes are expected, annealed for a reasonable time, then cooled down to room temperature. The Raman spectra in these experiments were always taken at room temperature (RT), after the indicated times from the beginning of the cooling process. The sequence of thermal treatments was the following.

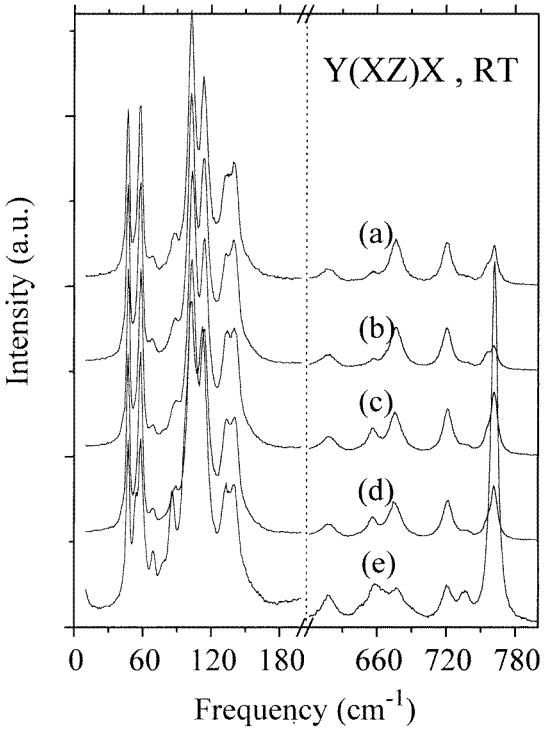

Figure 4. Comparison of the room-temperature Raman spectra in selected characteristic spectral ranges from Bi_2TeO_5 single crystals in the $Y(XZ)X$ polarization, due to different thermal annealings listed in table 2.

(a) Untreated crystal, reference spectra.
(b) Heating to 500 °C, annealing for 30 min and cooling to RT (3 hours).
(c) After process (b), heating to 600 °C, annealing for 30 min and cooling to RT.
(d) After process (c), 60 hours rest time at RT.
(e) After process (d), heating to 620 °C, annealing for 4 hours and cooling to RT (15 hours before measurement).

The data were systematically normalized in order to avoid artifacts due to any misplacement of the samples during heating and cooling. The reference lines for this normalization were selected for each polarization in a way that the majority of the Raman lines remained unchanged or the change was minimum. This concept resulted in a good overlap of the spectra after various heat treatments.

The general feature of the Raman spectra after the various thermal annealings is shown in figure 4. Data for the $Y(XZ)X$ polarization are depicted, after normalization on the 58 cm^{-1} line. As changes among the different processes occur particularly in two frequency regions of the spectra (from 10 to 200 cm^{-1} and 600 to 800 cm^{-1}), the central section of the spectra is not shown in the figure. The tendency of the changes in the Raman spectra after the various annealings was similar in the $Y(XY)X$ and $Y(ZY)X$ polarization arrangements but the intensity changes were less distinct. Only the Raman spectra in the $Y(ZZ)X$ polarization remained unchanged, within the experimental error, after the different heat treatments.

The most remarkable changes occurred after the last, 620 °C thermal treatment (spectrum

Table 2. Characteristic changes of 762 cm^{-1} structure in the Raman spectra of Bi_2TeO_5 single crystals as a function of various subsequent thermal annealings. All spectra were measured at room temperature after the heat treatment. Data were normalized to the peak intensity of the untreated sample for each polarization.

	Polarization			
Treatment	$Y(ZZ)X$	$Y(XY)X$	$Y(XZ)X$	$Y(ZY)X$
(a) Untreated	1	1	1	1
(b) 30 min at 500 °C	0.83	0.61	0.63	1.11
(c) 30 min at 600 °C	0.9	1.63	1.57	0.78
(d) 60 h at RT	0.87	1.59	1.37	0.64
(e) 4 h at 620 °C	0.87	10.58	8.91	10.41

(e) in figure 4). By comparing this spectrum with the spectra (a) to (d), one can notice the following.

(i) In the low-frequency range, the following lines have increased: 48, 53, 62 and 86 cm^{-1}. Also the strong lines at 101 and 112 cm^{-1} have increased and their relative intensities are modified.

(ii) In the high-frequency range, the lines at 618, 658, 721 and 735 cm^{-1} have increased. The most important increase, however, occurred at 762 cm^{-1}.

(iii) The spectral range from 200 to 600 cm^{-1} consists only of weak lines before and after annealing. Slight changes were detected in the 209, 231, 278, 344 and 512 cm^{-1} lines after the 620 °C treatment.

In the detailed analysis of the thermally induced changes, we will focus on the most characteristic spectral range from 650 to 800 cm^{-1}. Since the detailed thermal past of the crystals was unknown, the first thermal process might be a rearrangement of the residual excess oxygen that was captured in previous high-temperature oxidation (e.g. during crystal growth). The 500 °C annealing targeted this process (spectra (b)). The short 600 °C (spectra (c)) and the longer 620 °C (spectra (e)) annealing were expected to induce partial and more perfect oxidation to Bi_2TeO_6. The long rest period (spectra (d)) aimed to check the room-temperature oxygen loss from the oxidized samples. Consequently, the influence of the oxidation on the Raman spectra can be analysed mainly by comparison of Raman spectra (c), (d) and (e) with the spectrum (b).

Specific Raman lines were observed that were sensitive for the annealing mentioned above. As shown in figure 4, the most characteristic line was situated at 762 cm^{-1}. This line in the untreated crystal was very strong in the $Y(ZZ)X$ polarization but it was also observable in the $Y(XY)X$, $Y(ZY)X$ and $Y(XZ)X$ polarizations. Thermal annealing induced changes were predominant in the $Y(XY)X$, $Y(ZY)X$ and $Y(XZ)X$ polarization, where the original signal was weak at 762 cm^{-1}. Figures 5 and 6 show selected parts of the Raman spectra with these polarizations in the 650 to 800 cm^{-1} range. Only the (b), (c), (d) and (e) thermal treatment where the most comparable changes appear are reported. As all these spectra have been normalized with spectra obtained on the untreated sample, the intensities reported in figures 5 and 6 are comparable. The relative changes of the peak intensity of the 762 cm^{-1} line are comparatively collected in table 2.

The first heating to 500 °C decreased the 762 cm^{-1} peak in the $Y(XY)X$, $Y(ZZ)X$ and $Y(XZ)X$ polarizations while in the $Y(ZY)X$ polarization the peak significantly increased (10%). In the $Y(ZZ)X$ polarization, this structure intensity is almost unchanged by the

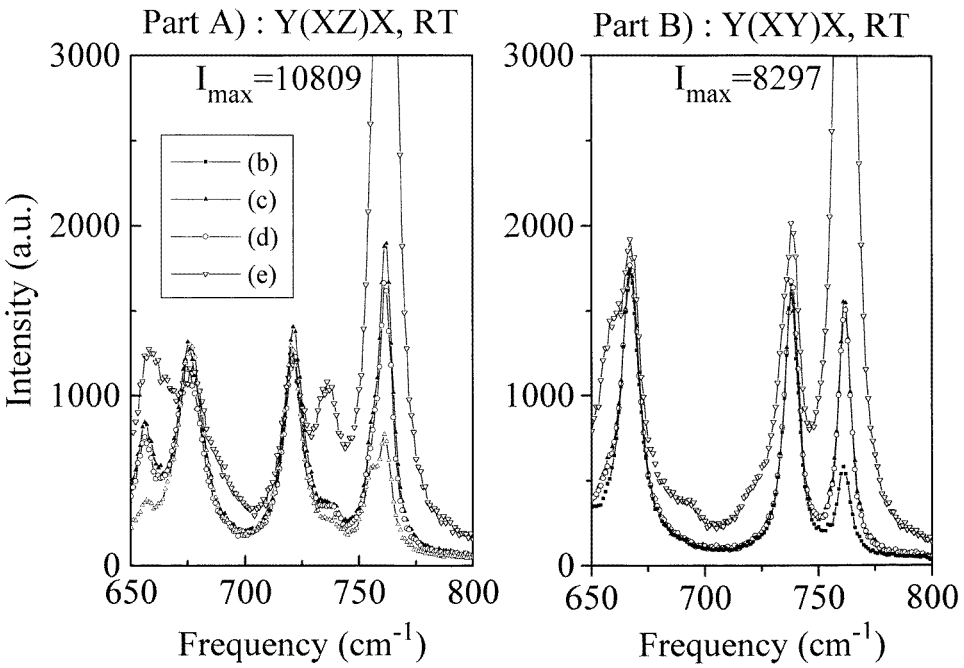

Figure 5. Characteristic changes in the room-temperature Raman spectra of Bi_2TeO_5 single crystals in the $Y(XZ)X$ (part A) and $Y(XY)X$ (part B) polarizations due to different thermal annealings listed in table 2. The spectra were normalized at 58 cm^{-1} and 69 cm^{-1}, respectively. (b), (c), (d) and (e) are marked by filled squares, filled up triangles, open circles and open down triangles, respectively.

other thermal treatment; in contrast the line intensity is strongly modified by the annealing process: the 600 °C annealing (c) enhanced the 762 cm^{-1} peak in all three orientations and the subsequent, long, room-temperature rest (d) only slightly reversed these changes. A dramatic increase of the peak was induced by the long 620 °C annealing (e) for the first three orientations but not for the $Y(ZZ)X$ symmetry vibration.

Similar but less pronounced changes were observed at the 658 cm^{-1} peak. This peak was strong in the $Y(ZY)X$ polarization and the changes could only be followed throughout the different annealings in the $Y(XY)X$ and $Y(XZ)X$ polarizations. After the 620 °C annealing, dramatic changes were observed in the whole Raman spectra and new peaks appeared in each polarization. The detailed analysis of these results will be the topic of a separate paper.

5. Discussion of the thermal annealing

The observations made in the literature [13, 14] and recent thermoanalytical data [16] indicated that filling of the empty oxygen position was efficient above 600 °C. The strong enhancement of the 762 cm^{-1} Raman line in the $Y(XY)X$, $Y(ZY)X$ and $Y(XZ)X$ polarization at matching temperatures appeared to be a good trace for this oxidation process. Since the 762 cm^{-1} line is strong and nearly unchanged in the $Y(ZZ)X$ symmetry polarization, the changes observed in the other asymmetric polarizations were due to an angular displacement of the existing vibration group rather than to the appearance of a new vibration. The Bi_2TeO_5 crystal structure contains two different types of open oxygen

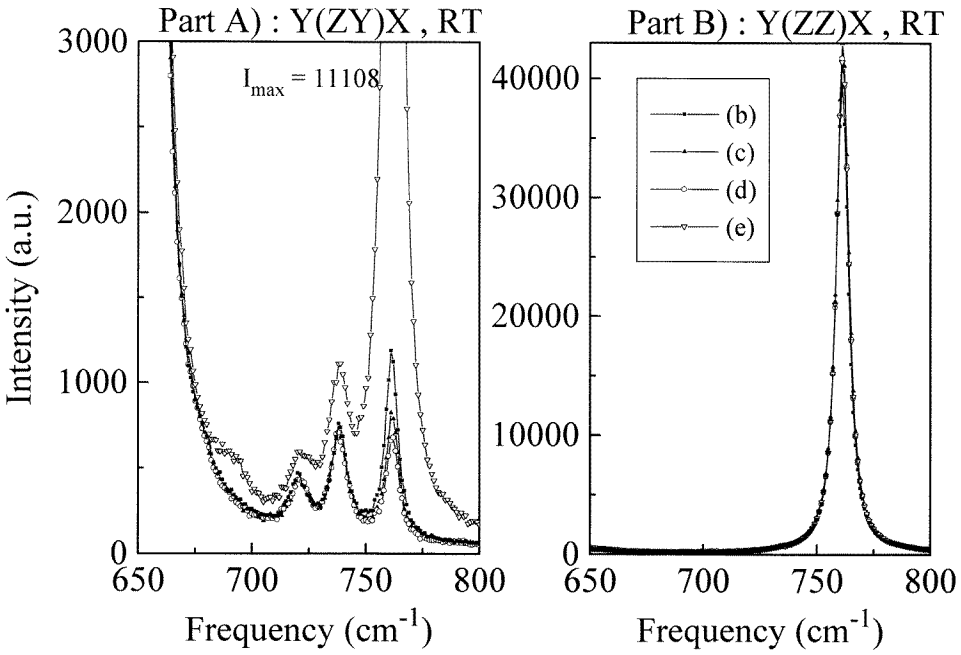

Figure 6. Characteristic changes in the room-temperature Raman spectra of Bi_2TeO_5 single crystals in the $Y(ZY)X$ (part A) and $Y(ZZ)X$ (part B) polarizations, due to different thermal annealings listed in table 2. The spectra were normalized at 76 cm^{-1} and 110 cm^{-1}, respectively. The same drawing symbols are used as in figure 5.

position [4]. One Bi atom is surrounding by eight oxygens, forming a strongly distorted cube. The two other Bi atoms are essentially bonded to seven oxygens. The tellurium is bonded with three oxygens, the Te–O bond being around 1.85 Å. The two other oxygens around Te are spaced from 3.07 Å and 3.24 Å. One orbital of the Te is free. The fact that any changes appear in $Y(ZZ)X$ symmetry polarization may be due to the great symmetry of the corresponding mode A_1. The annealing processes can create oxygen oscillations but do not change the global polarization and consequently the Raman spectra. In the other symmetry configurations, the changes in Raman spectra could be due to an occupation of the Te free orbital by an oxygen.

From inside the sublattice of four Te, both oxygens are missing. The local charge compensation is given by the lone electron pairs of the tellurium ions that are directed to the empty oxygen sites. These Te orbitals are in bonds with oxygen when the Te has 6^+ nominal charge. In the sublattice of 3 Bi and 1 Te, there is a single oxygen vacancy, while the other sublattices (4 Bi, 2 Bi + 2 Te) are fully occupied. From the point of view of filling with oxygen, the two types of vacancy site provide three options; the lone vacancy, the first and the second occupations of the vacancy pair. These options may be different energetically and kinetically. In this picture, a single-step oxidation appears to be only a rough approximation. The trace line at 762 cm^{-1} in the Raman spectra may relate to any of the options mentioned above. The double occupancy in the untreated crystal, however, is unlikely.

The stability of the oxygen excess related spectra at room temperature (measurement (d)) indicated that the oxygen loss from the oxidized state was kinetically blocked. Consequently,

the as-grown Bi_2TeO_5 crystals may contain some excess oxygen too. The intensity of the 762 cm^{-1} Raman line in the $Y(XY)X$ and $Y(XZ)X$, and less effectively in the $Y(ZY)X$ directions seems to be a good indication for residual excess oxygen. Annealing of the crystals in the 400–500 °C range partially mobilizes this excess oxygen. The observed decrease of the 762 cm^{-1} line at these temperatures is attributed to the oxygen migration away from the Raman active centre.

6. Conclusion

Raman spectra of Bi_2TeO_5 were taken at different temperatures and for four polarizations. The variation of the different-frequency line structures has been analysed as a function of the temperature. It was shown to remain almost constant in the range from 10 K to 600 °C which is clearly indicative of the absence of a phase transition.

Specific Raman lines were found that were sensitive for the thermal history of the crystals. The characteristic temperatures for spectral changes were in good agreement with the literature data for oxidation and oxygen loss (Bi_2TeO_5–Bi_2TeO_6 system). The reduction to Bi_2TeO_5 in the cooling process was slow; the room-temperature crystals might contain various amounts of excess oxygen. This is a possible reason for the peculiarities observed in various different physical investigations. We recommend testing the actual oxidation status of the samples by measuring the intensity of the 762 cm^{-1} Raman line in the $Y(XZ)X$ polarization.

Acknowledgments

The authors want to express their gratitude to the ESF Network on Oxide Crystals, French–Hungarian joint Research Fund, BALATON, Hungarian Research Fund, and OTKA grant T-014884 for their support, to Mrs I Perczel for her contribution in crystal growth and Mrs Á Péter and Mr Gy Matók for their work in crystal processing and characterization.

References

[1] Földvári I, Scripsick M P, Halliburton L E and Péter Á 1991 *Phys. Lett.* **154A** 84
[2] Földvári I, Liu H, Powell R C and Péter Á 1992 *J. Appl. Phys.* **71** 5465
[3] Péter Á, Szakács O, Földvári I, Bencs L and Munoz A 1996 *Mater. Res. Bull.* **31** 1067
[4] Földvári I, Péter Á, Voszka R and Kappers L A 1990 *J. Cryst. Growth* **100** 75
[5] Dolgikh B A, Demina L A, Stefanovich S Yu, Popovkin B A, Vorobeva O I and Kucheryavenko S I 1985 *Inorg. Mater.* **21** 399
[6] Simon A *et al* 1979 *Solid State Commun.* **29** 815
[7] Stefanovich S Yu, Sadovskaya L Ya and Antonenko A M 1991 *Sov. Phys.–Solid State* **33** 1249
[8] Avramenko V P *et al* 1990 *Bull. Acad. Sci. SSSR Ser. Phys.* **54** 184
[9] Földvári I, Kappers L A and Powell R C 1997 *Mater. Sci. Forum* **239–241** 315
[10] El Farissi M, Mercurio D and Frit B 1987 *Mater. Chem. Phys.* **16** 133
[11] Mercurio D, Parry B H, Frit B, Harburn G, Williams R P and Tilley R J D 1991 *J. Solid State Chem.* **92** 449
[12] Mercurio D, El Farissi M, Frit B and Goursat P 1983 *Mater. Chem. Phys.* **9** 467
[13] Gospodinov G and Gyurova K 1985 *Thermochim. Acta* **83** 243
[14] Frit B and Jaymes M 1974 *Bull. Soc. Chim. France* **3/4** 402
[15] Rousseau D L, Bauman R P and Porto S P S 1981 *J. Raman Spectrosc.* **10** 255
[16] Pöppl L 1997 private communication